Experimental Combustion Analysis in a Gasoline Baseline Hydrogen-Fueled Internal Combustion Engine at Ultra-Lean Conditions

Caio Ramalho Leite, Mathieu Laignel, Pierre Brequigny, Jacques Borée, Fabrice Foucher

Experimental combustion analysis in a gasoline baseline hydrogen-fueled internal combustion engine at ultra-lean conditions

Caio Ramalho Leite, Mathieu Laignel, Pierre Brequigny
Université d'Orléans, France

Jacques Borée
ENSMA, France

Fabrice Foucher
Université d'Orléans, France

ABSTRACT

Hydrogen-fueled internal combustion engines (H_2ICEs) have emerged as a promising technology for reducing greenhouse gas emissions in the transportation sector. However, due to the unique properties of hydrogen, especially under ultra-lean conditions, the combustion characteristics of hydrogen flames differ significantly from those of conventional fuels. This research focuses on evaluating the combustion process and cycle-to-cycle variations (CCVs) in a single-cylinder port-fuel injection H_2ICE, as well as their impact on performance parameters. To assess in-cylinder combustion, three indicators of flame development are utilized and compared to the fundamental properties of hydrogen. The study investigates the effects of various factors including fuel-air equivalence ratio (ranging from 0.2 to 0.55), engine load (IMEP between 1 and 4 bar), and engine speed (900 to 1500 rpm). The analysis aims to understand the behavior of the flame initiation phase, which refers to the time from ignition to 10% of the mass fraction burned, as it is found to be the most sensitive period of combustion duration in H2ICEs with respect to the fuel-air equivalence ratio. The research reveals that within a wide range of equivalence ratios, there is minimal variability in combustion. The study also discusses the characteristics of the flame at ignition timing, considering the influence of factors such as turbulence and thermodiffusive instabilities. To aid in the analysis, 0D/1D engine simulations are employed, providing valuable insights into the underlying mechanisms shaping the flame behavior.

INTRODUCTION

Hydrogen is being considered as a potential substitute for fossil fuels in internal combustion engines (ICEs) due to its potential for zero-carbon emissions and energy supply security [1, 2]. Recent studies have shown that ultra-lean hydrogen-air mixtures (with a fuel-air equivalence ratio from 0.2 to 0.5) could be an effective strategy to reduce NOx emissions in hydrogen-fueled spark-ignition engines (H_2ICE) [1].

However, it is well-known that decreasing the equivalence ratio leads to higher engine instability and greater cycle-to-cycle variations (CCVs) [3]. Despite this, hydrogen flames exhibit thermodiffusive (TD) instabilities, particularly at low equivalence ratios and high pressures. These instabilities can accelerate combustion and significantly alter flame development, potentially affecting its variability under ICE operating conditions [4, 5, 6].

Some previous studies have investigated cycle-to-cycle variations (CCVs) in hydrogen-fueled internal combustion engines (H2ICEs) using both direct-injection (DI) and port fuel injection (PFI) systems [7, 8, 9, 10, 11]. However, the majority of these studies focused on close-to-stoichiometric mixtures. For instance, Kim et al. [7] found that the decrease in equivalence ratio is associated with an increase in CCVs, primarily due to variations in the flame initiation process, which is in contrast to gasoline engines. Ma et al. [8] and Li et al. [9] demonstrated that combustion instabilities increase at lower loads and fuel-air equivalence ratios. Chen [10] examined the performance of PFI hydrogen-fueled engines at idle conditions and found that hydrogen injection timing has minimal effect on CCVs. On the other hand, Sun et al. [11] showed that combustion instability is heightened in lean/ultra-lean conditions, and the ignition timing significantly

influences CCVs in ultra-lean mixtures, with the lowest variations observed at MBT (maximum brake torque), a finding also supported by Li et al. [9]. However, it is important to note that the use of ultra-lean hydrogen-air mixtures at high in-cylinder pressures during spark timing leads to inherently unstable flames [12]. Therefore, further research is necessary to analyze and understand the behavior of hydrogen flames under these specific engine conditions.

Given that these engine conditions are relatively new and limited data is available in this area, such as heat transfer models and wall temperature boundary conditions, it is crucial to adopt a comprehensive strategy to address these uncertainties effectively. One approach that has gained prominence is the use of Three Pressure Analysis (TPA) with a 0D/1D two-zone engine simulator, which enable the analysis of experimental results and extraction of unknown data from the in-cylinder pressure trace and other experimental conditions. By utilizing such simulators, researchers can enhance their understanding of the combustion process and gain insights into the complex phenomena occurring within the engine [13, 14, 15, 16, 17].

The main focus of this study is to experimentally investigate the combustion of hydrogen and the cyclic variations on gasoline baseline retrofitted H_2ICEs with a TPA analysis strategy. It aims to gain an understanding of ultra-lean/lean hydrogen combustion under tumbling flows and to evaluate key parameters affecting flame development and CCVs under these conditions. A cyclic variability analysis is conducted by sweeping the equivalence ratio within the range of 0.175 to 0.55, considering four different indicated mean effective pressures (IMEPs) ranging from 1 to 4 bar. Furthermore, constant intake pressure and spark timing studies are carried out with an equivalence ratio range of 0.25 to 0.55, while varying the engine speed at 900, 1200, and 1500 rpm. These investigations aim to provide insights into the combustion physics of hydrogen within the combustion chamber, allowing for a better understanding of its behavior under different operating conditions.

The results obtained from this study could be beneficial in the mid-term by facilitating the adaptation of current gasoline engines for hydrogen use to reduce carbon emissions, and in the long-term, by providing experimental and fundamentals knowledge on hydrogen combustion for the development of more efficient hydrogen engine architectures.

EXPERIMENTAL SETUP AND METHODOLOGY

A single-cylinder, four-stroke, optical spark-ignition engine was used to conduct the experiments. It has a pent-roof cylinder head and a bowl-type piston. The setup scheme can be found in Figure 1 and a summary of the main parameters in Table 1.

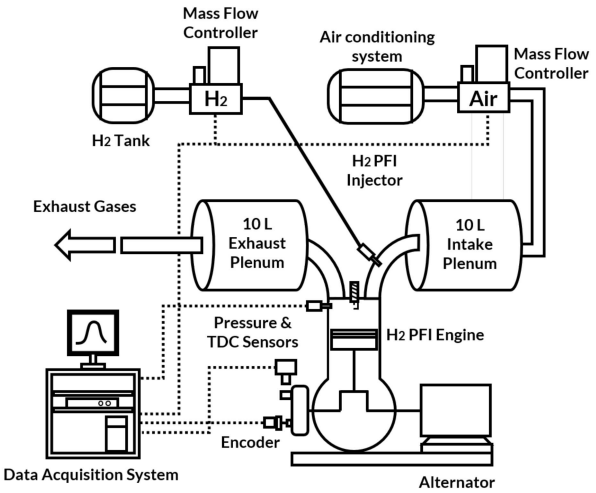

Figure 1: Hydrogen-fueled engine experimental scheme.

The cooling water is heated up to 85 °C and maintained at a temperature below 90 °C during the experiments. Prior to entering the intake plenum, the intake air is filtered for particles and oil, and dehumidified. To maintain consistent and controlled intake conditions, a closed-loop control system is utilized to regulate the intake pressure. Simultaneously, the exhaust line is vented to atmospheric pressure. Temperature measurements along the intake and exhaust lines are obtained using K-type thermocouples, providing data for monitoring and analysis purposes.

The parameters are adjusted via an in-house LabView control system. The engine is coupled with an electric motor to allow for motoring operations between 600 and 1900 rpm. An optical encoder guarantees the recording of 100 cycles with a 0.1 CAD increment. Continuous hydrogen injection into the intake pipe is utilized to achieve a more homogeneous mixture.

In-cylinder pressure is measured using an AVL QH32C piezoelectric sensor (with a precision of $\pm$ 0.2% FSO), while intake and exhaust

Table 1: Parameters of the 0.4 L hydrogen engine. Crank Angle Degrees (CAD) are relative to the firing Top-Dead Center (0 °aTDC). The CAD of valve openings and closures correspond to experimental residual valve lifts of 0.1 mm.

Engine model	**PSA Optical EP6**
Number of cylinders	1
Cylinder head	Pent-roof
Piston	Bowl type
Injection type	PFI (Homogeneous)
Bore	77 mm
Stroke	85.8 mm
Compression Ratio	10.5
Connecting rod length	138.5
Piston-to-Crank Offset	0.8 mm
Intake valve open	+357 °aTDC
Intake valve close	−122 °aTDC
Exhaust valve open	+141 °aTDC
Exhaust valve close	−339 °aTDC

pressures (P_2 and P_3, respectively) are obtained from Kistler 4075A piezoresistive sensors ($< \pm$ 0.1% FSO). Airflow is measured with a Micro Motion F025S Coriolis meter, and hydrogen mass is controlled by an Emerson 5850S mass flow controller. The flow meters for hydrogen and air mass flow were calibrated before conducting the experiments. The measurement accuracy for hydrogen mass flow is 0.7% of the flow rate, while for air mass flow, it is 0.5%.

The experimental setup displayed in Figure 2 includes intake and exhaust ducts with a diameter of 40 mm. The hydrogen injection takes place in a 6 mm diameter duct located 600 mm away from the cylinder head at the center of the intake duct.

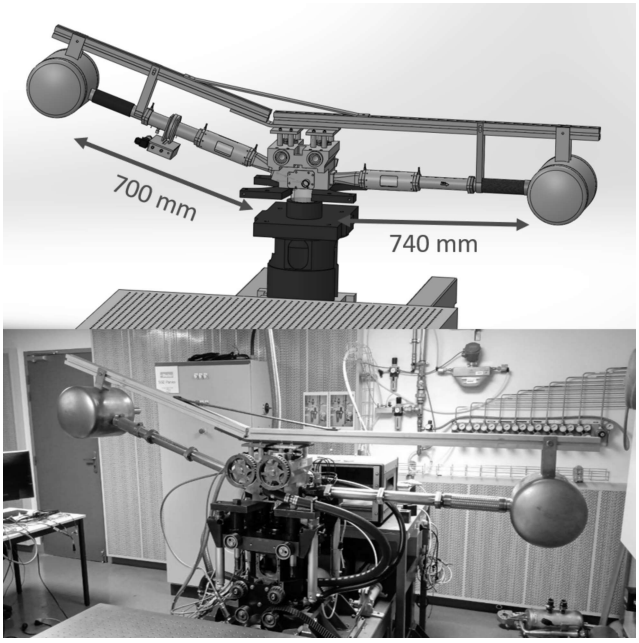

Figure 2: Optical hydrogen-fueled engine experimental bench.

The combustion performance parameters were evaluated by varying the equivalence ratio, engine speed, and load, as detailed in Table 2. To assess engine stability, the coefficient of variation of IMEP (CoV_{IMEP}) was used, while the combustion duration ($\Delta\theta$), calculated using the heat release rate (HRR) equation, was used to analyze the combustion process and flame variability.

Table 2: Experiments methodology.

Parameter	**Sensibility study**
Equivalence ratio	$0.2 < \phi < 0.55$
Load	IMEP = 1, 2, 3, and 4 bar
Engine speed	900, 1200, and 1500 rpm
Intake pressure	0.7 and 0.9 bar

NUMERICAL MODEL

Given that the combustion analysis heavily relies on the accuracy of the heat transfer model, and considering that hydrogen combustion heat transfer models are still under development [18], the investigation utilized GT-Power (Gamma Technologies), a 0D/1D simulator. This simulator was employed to extract important in-cylinder conditions with the two zones approach, including unburned temperature, burned temperature, mass trapped, and more, by analyzing the in-cylinder, intake port, and exhaust port pressures [14].

The model was developed using the Three Pressure Analysis (TPA) method, which utilizes measured dynamic pressure profiles (namely intake, exhaust, and cylinder) to calculate the combustion rate. The measured high-speed intake and exhaust pressure curves are set as input conditions for the simulation. A TPA model is constructed by incorporating engine components such as ports, runners, valves, cylinder, and engine crank train geometry to estimate cylinder conditions. Details such as valve lifts and discharge coefficients are also required for this approach [13].

The TPA method is employed to conduct two types of experimental analysis: ensemble-averaged and multiple consecutive cycle. The former is used to examine cycle-to-cycle variations, while the latter provides average operating conditions over 100 cycles. In both cases, the intake and exhaust port boundaries are imposed from an instantaneous pressure trace measurement, and the calculated apparent burn rate is fitted for combustion parameters prediction [13].

The engine, intake ports, and exhaust ports were designed in the software, as shown in Figure 3. The numerical model incorporates the measured intake and exhaust valve lifts and discharge coefficients. Figure 4 illustrates an example of the imposed pressure traces and valve lifts.

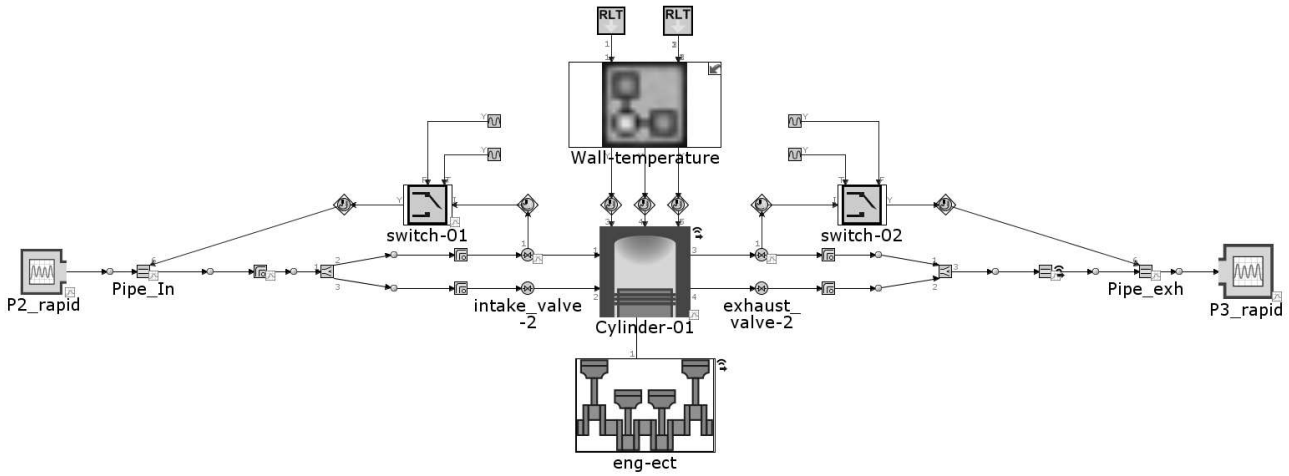

Figure 3: Three pressure analysis model for the EP6 optical engine.

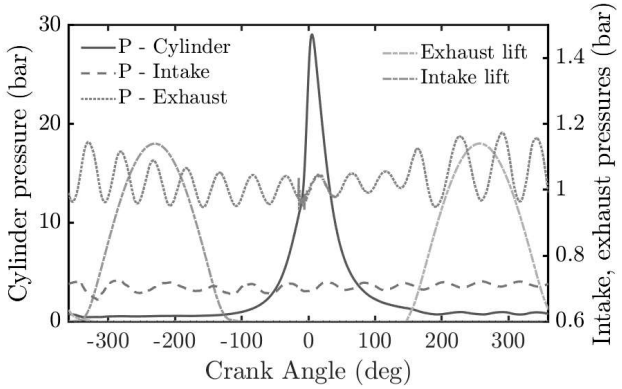

Figure 4: An example of ensemble-averaged cylinder, intake, and exhaust pressure curves, as well as intake and exhaust valve lifts, operating at 1200 rpm, ϕ = 0.55, P_2 = 0.7 bar, and spark timing at -15 °aTDC.

Once the pressure inputs and geometry are configured, the next step is to establish the boundary conditions. Achieving accurate results with the TPA method requires a close match between the simulated cylinder pressure traces and the measured cylinder pressure profile.

To accomplish this, the engine compression ratio and the heat transfer within the combustion chamber are crucial inputs. Specifying the wall temperatures of the ports and of the combustion chamber is necessary to obtain an accurate estimation of the volumetric efficiency and heat transfer.

Since detailed information about the cooling system and heat transfer coefficients for each component is limited, a model that estimates the heat flux absorbed by the cooling water and by the wall material was used to calculate the wall temperature of the cylinder head, cylinder, and piston. This model follows a similar approach to the "EngCylTWallSoln" template in GT-Power [13]. For the intake and exhaust ports, the wall temperature is imposed as the same temperature of the cylinder head.

The heat transfer inside the cylinder is calculated using the Woschni equation for tumble flow [19]. A constant in-cylinder heat transfer convection multiplier is adjusted for each operating condition, aiming to match the gross indicated effective pressure (gIMEP) and the in-cylinder pressure trace. The GT Direct Optimizer tool is employed to minimize the relative error between the experimental data and the simulation results. The heat transfer multiplier is allowed to vary between 1 and 3 [14].

To evaluate the effective compression ratio, a simulation is conducted using two experimental points in motoring conditions. For this simulation, the heat transfer convection multiplier is set to 1. A design of experiments (DoE) is then performed based on the geometric compression ratio of 10.5:1. The effective compression ratio is varied between 9.4:1 and 10.4:1. The in-cylinder pressure as a function of the crank angle is obtained for the two experimental conditions described in Table 3, as well as for the simulation results using six compression ratios for each reference condition. Figure 5 presents the in-cylinder pressure traces for these cases. It is observed that the measured cylinder pressure matches well with a compression ratio of 9.8:1 for both motoring references. Therefore, the compression ratio of 9.8:1 is kept constant for all the experimental points studied.

Table 3: Two motoring reference points.

Engine speed	$\mathbf{P_2}$	$\mathbf{P_3}$	**T2**
1200 rpm	0.7 bar	1 bar	23 °C
1200 rpm	0.9 bar	1 bar	23 °C

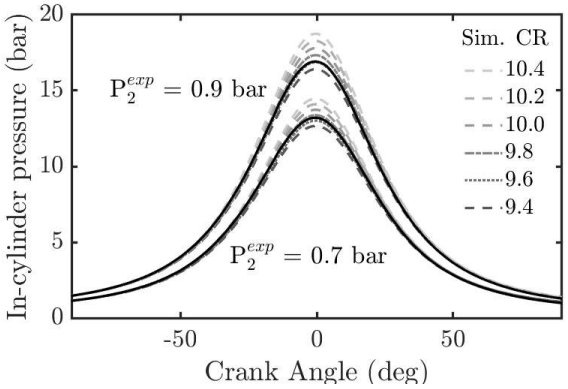

Figure 5: Effective compression ratio study for two motoring reference cases.

The model was validated for hydrogen combustion across a range of equivalence ratios (from 0.25 to 0.55), mean intake pressures (0.7 and 0.9), spark timings (from -87 to -15 °aTDC), and engine speeds (900, 1200, and 1500 rpm). The validation process involved comparing the simulated results with the measured values for two key parameters: (a) mass flow rate at the intake, which provides insights into volumetric efficiency and in-cylinder trapped mass, and (b) gIMEP, which indicates the work done throughout the cycle. The relative errors between the simulated and measured values were found to be within a range of 5% for the total mass flow rate and 1% for gIMEP, as shown in Figures 6 and 7.

Additionally, Figure 8 presents a comparison between the ensemble-averaged measured and simulated cylinder pressure traces for two different operating conditions: 4 bar of IMEP, spark timing at -45 °aTDC, and an equivalence ratio of 0.25; and 3 bar of IMEP, spark timing at -7 °aTDC, and an equivalence ratio of 0.55. Despite the experimental points exhibiting different pressure traces, the simulation accurately captures the behavior inside the cylinder. The analysis revealed that the heat transfer convection multiplier ranges from 2.8 to 1.3 in all simulation cases. This indicates that the overall Woschni equation underestimates the heat transfer for hydrogen. Interestingly, the highest values of the convection multiplier are observed at low equivalence ratios, and as the fuel-air equivalence ratio increases, the values decrease and approach 1. This implies that ultra-lean hydrogen combustion deviates more from the Woschni equation compared to mixtures closer to stoichiometry.

As hydrogen-air mixtures exhibit distinct behavior compared to conventional fuels, particularly under ultra-lean conditions, conducting

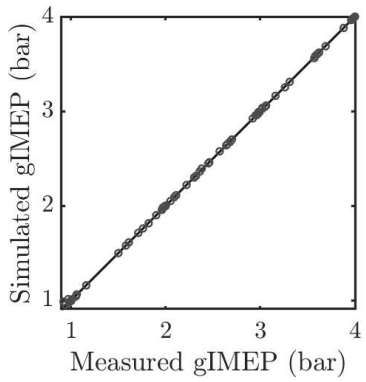

Figure 6: Gross Indicated Mean Effective Pressure (gIMEP) relative error between experiment and simulation for all conditions.

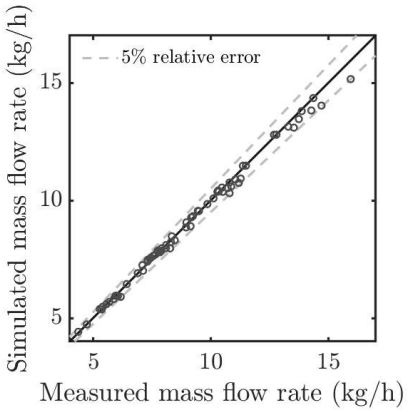

Figure 7: Mass flow rate relative error between experiment and simulation for all conditions.

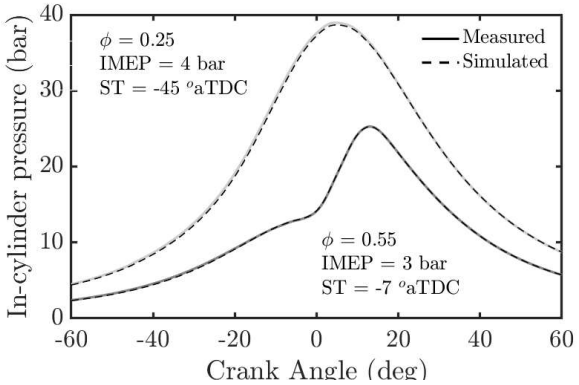

Figure 8: Simulated and measured pressure traces for two experimental conditions.

a rigorous post-treatment analysis of experimental data becomes crucial. For instance, the heat transfer model significantly influences the net heat release, which, in turn, affects the calculation of the mass fraction burned and the subsequent analysis of the combustion process. Therefore, it is essential to have a comprehensive understanding of the key parameters influencing the flame behavior in the upcoming study.

RESULTS AND DISCUSSION

CYCLE-TO-CYCLE VARIATION ANALYSIS The first experiment aims to investigate the influence of the equivalence ratio in the engine cyclic variations at different loads (idling and low loads). It is done varying the fuel-air equivalence ratio while targeting four IMEP values (1, 2, 3, and 4 bar), with optimized spark timing to maximize efficiency and torque. The coefficient of variation (CoV), a metric used to measure engine stability, is calculated by dividing the standard deviation by the mean over 100 cycles.

Figure 9 illustrates the relationship between CoV (in percentage) and fuel-air equivalence ratio for all IMEP values. It indicates that the coefficient of variation of IMEP increases as the equivalence ratio decreases, which is expected. However, the increase is not significant enough to exceed the stability limit of 4%. This is noteworthy because flame properties, such as the laminar flame speed and adiabatic flame temperature, significantly change between these equivalence ratios. The engine remains stable until ϕ = 0.2 (λ = 5), but misfires occur for all loads with leaner mixtures.

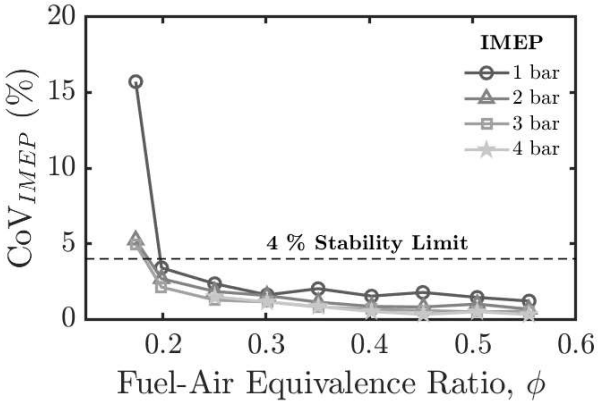

Figure 9: Equivalence ratio and load effects on engine stability.

Furthermore, it is worth noting that the CCVs increase as the load decreases, which is in agreement with the literature [20, 7]. For the same equivalence ratio, an IMEP of 4 bar can be up to 5 times more stable than an IMEP of 1 bar (at ϕ = 0.45). Since idling (IMEP = 1 bar) is the lowest load expected in an internal combustion engine for the transport application, this condition does not appear to have enough CCVs to cause operating instabilities.

To gain insight into why cyclic variations are not occurring over this wide range of equivalence ratios, it is important to analyze the combustion durations under these operating conditions.

Figure 10 illustrates the effect of equivalence ratio and load on the duration of three flame phases: at the top, the flame initiation phase (from spark ignition to 10% of mass fraction burned - MFB); below, the flame propagation phase (from 10 to 50% of MFB); and the third graph, the end-flame phase (from 50 to 90% of MFB). At the bottom, the total combustion duration (from 10 to 90% of MFB) is also displayed.

The flame initiation phase is the most affected by the equivalence ratio sweep, followed by the flame propagation and the end-flame phases, respectively. Additionally, the flame initiation phase exhibits a second-order trend with respect to the equivalence ratio, while the combustion duration from 10 to 50% MFB shows almost a linear trend, and the end-flame phase shows a quasi-constant trend of around 30 crank angle degrees (CAD). The combustion duration increases from +50% (22 to 31 CAD) at the end-flame phase (IMEP = 3 bar) to +211% (6.5 to 21.5 CAD) at the flame propagation phase (IMEP = 2 bar), and up to +370% (9 to 42 CAD) at the initiation phase (IMEP = 2 bar) as the equivalence ratio decreases from 0.55 to 0.2.

Furthermore, Figure 10 shows that the flame initiation duration is the most sensitive flame phase to load variations (i.e., intake pressure). A difference in load from 1 to 4 bar (e.g., 0.5 to 1.05 bar of intake pressure) can increase the combustion speed by 6 CAD at ϕ = 0.35 and by more than 10 CAD at ϕ = 0.2, when IMEP increases from 1 to 3 bar (and intake pressure from 0.74 to 1.3 bar). The end-flame, on the other hand, exhibits a seemingly load-independent behavior.

The flame initiation is found to be the critical phase in the flame development and, thus, in H_2ICE performance, as already seen with swirled based geometry [6]. However, it is not possible to draw definitive conclusions about the flame from a constant IMEP experiment since many parameters affecting it, such as intake pressure, equivalence ratio, and spark timing, are varying. Therefore, to better understand the combustion physics of hydrogen in an ICE, another experimental analysis is needed.

HYDROGEN FLAME FUNDAMENTALS ANALYSIS In order to study the impact of equivalence ratio, turbulence, and pressure at the spark timing on the hydrogen flame, an analysis was conducted in which intake pressure and spark timing were kept fixed to ensure similar thermodynamic conditions at the moment of the spark. Equivalence ratio, which impacts the flame dynamics, and engine speed, which affects turbulence, were varied for two intake pressures. Figure 11 displays the variation of in-cylinder pressure (from the experiments and from the TPA simulation) and mass fractions burned with crank angle for different equivalence ratios at a constant engine speed of 900 rpm and intake pressure of 0.7 bar. By analyzing the in-cylinder pressure trace, it is evident that as the equivalence

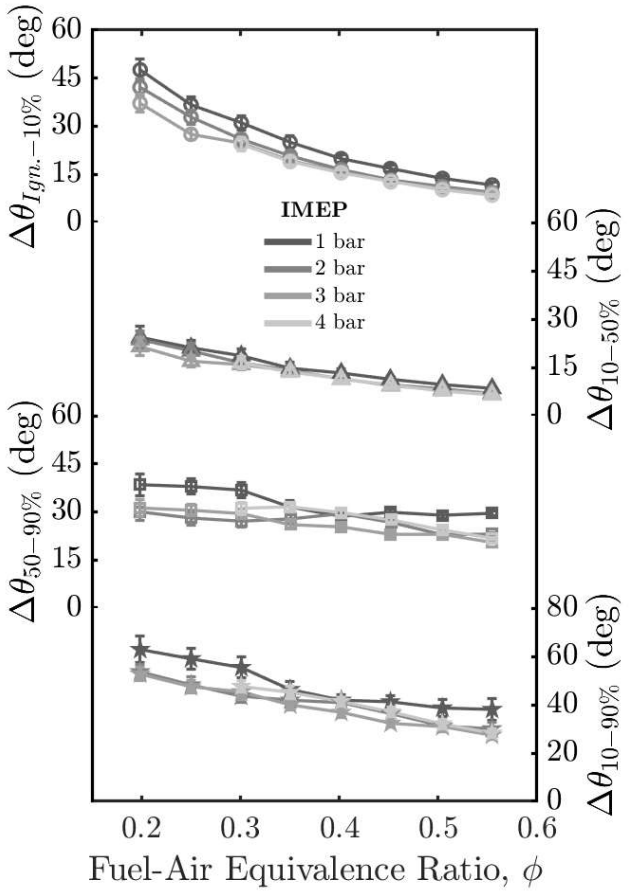

Figure 10: Combustion duration of the flame initiation (first), flame propagation (second), end-flame (third), and total, 10 to 90% (fourth), as a function of the equivalence ratio for the ϕ and IMEP sweep.

ratios increase, the heat release also increases while the combustion duration decreases. This can be observed by the crank angle where the maximum pressure occurs, which approaches the spark timing. This reasoning is supported by the bottom graph, where the combustion durations can be found for each equivalence ratio. The difference in combustion duration (from 10 to 90% of MFB) decreases from 73.9 CAD for ϕ = 0.25 to 27.1 CAD for ϕ = 0.55. The flame initiation duration also undergoes significant alterations. Besides, the simulations closely match the experimental results for all the cases studied. Since the simulated in-cylinder pressure is used to calculate heat release, unburned temperatures, and mass fraction burned, a more accurate calculation of parameters is performed. Therefore, all the data presented from this point onward refer to the TPA simulations.

Moreover, the engine speed is varied in the range of 900 to 1500 rpm. Figure 12 presents the in-cylinder pressure and mass fraction burned profiles for three different engine speeds at ϕ = 0.45 and an intake pressure of 0.7 bar. It should be noted that since the spark timing is not adjusted to optimize the burning time, the comparison primarily focuses on the flame initiation phase, where the thermodynamic conditions are closer to real engine applications. The differences observed in the flame development as depicted in Figure 12, more evident at the mass fraction burned graph, will be analyzed across all equivalence ratios, engine speeds, and intake pressures using the combustion duration from spark timing to 10% of MFB as a key metric. The slow development of the flame kernel, which differs approximately 5 CAD, from the highest engine speed compared to the lowest one in this case, will be further analyzed using turbulent flame modeling equations.

The combustion duration from spark timing to 10% of MFB was calculated for all the experiments conducted. Figure 13 illustrates this duration for the three engine speeds tested with P_2 = 0.7 bar. The trend observed indicates that the burning angle during the flame initiation period decreases as the equivalence ratio increases. This behavior can be attributed to the corresponding increase in the laminar flame speed under these operating conditions. The increase in equivalence ratio from 0.25 to 0.55 resulted in a decrease in the burning angle from 26.6 to 8.1 CAD (at 900 rpm), 9.1 CAD (at 1200 rpm), and 10.5 CAD (at 1500 rpm), corresponding to a reduction of up to 69.5%.

Furthermore, during the early stages of flame development, there is a similar duration (measured in crank angle degrees) for all rotation speeds when considering fuel-air equivalence ratios below 0.35. Thus, although the crank angles may not represent the same physical

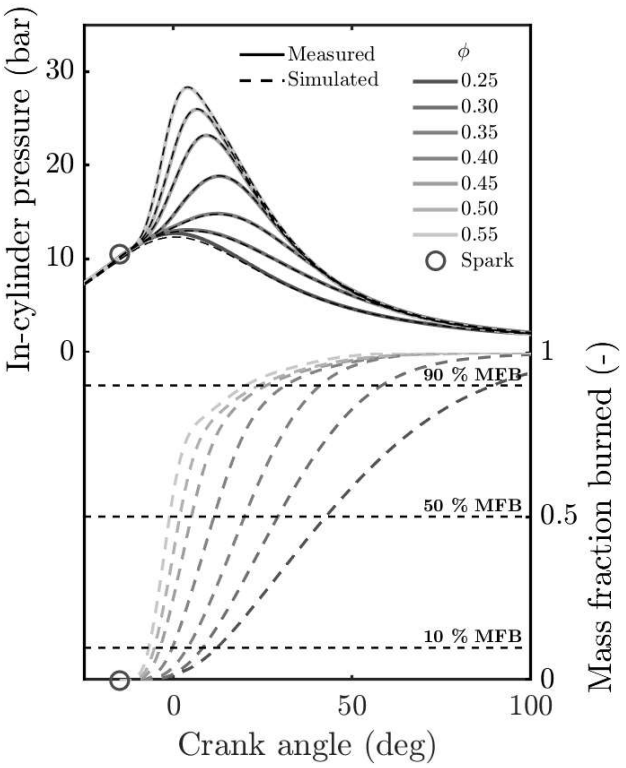

Figure 11: In-cylinder pressure and mass fraction burned as a function of the crank angle for 7 equivalence ratios at 900 rpm and P_2 = 0.7 bar. The spark timing is -15 °aTDC.

time, the presence of turbulence affects the flame speed in a way that allows all flames to burn within the same amount of crankshaft rotation angle. However, at higher equivalence ratios, the burning time between these conditions starts to vary. The combustion duration at 900 rpm occurs in fewer crank angle degrees compared to 1500 rpm, indicating that turbulence has a lesser impact on the burning speed at higher equivalence ratios. Instead, the primary influence is attributed to fundamental flame properties, such as the laminar flame speed. Since the laminar flame speed remains the same at a given pressure, temperature and equivalence ratio for all rotation speeds, a flame at higher rotation speeds would require more crank angle degrees to complete the burning process.

To gain a deeper understanding of the flame behavior in these experimental conditions, it is necessary to analyze the changes in burning aspects from a perspective of physical time. Figure 14 presents the same experimental results as Figure 13, but with the y-axis representing burning time in milliseconds, $t_{\Delta\theta}$. As expected, the burning time for flame initiation decreases with increasing equivalence ratio for all engine speeds, primarily due to the higher laminar flame speed of hydrogen-air mixtures. However, the rate of decrease is not consistent across all turbulence conditions. As previously hypothesized, the burning time for the flame kernel development from spark timing to 10% of MFB becomes increasingly dependent on flame properties as the equivalence ratio rises. This trend is evident in the graph, as the burning times for all speeds tend to converge at higher equivalence ratios. In contrast, at lower equivalence ratios, there is a noticeable difference in the burning time during the initial flame phase among different engine speeds, confirming the hypothesis that turbulence plays a significant role in flame development under these conditions.

To account for the influence of turbulent intensity and isolate the flame propagating properties, an analysis of the burning time considering the laminar flame speed properties is conducted. For this purpose, a characteristic flame time, denoted as t_f, is introduced. It is defined as the ratio of the laminar flame thickness (δ_L) to the laminar flame speed (s_L^0) ($t_f = \frac{\delta_L}{s_L^0}$). In order to determine the values of these flame properties, calculations are performed with the CONVERGE CFD Software [21] using three hydrogen-air kinetic mechanisms: Burke et al. [22], Alekseev et al. [23] and GRI-Mech 3.0 [24] under the spark timing conditions.

Figure 15 presents the laminar flame speed and thickness obtained from the equivalence ratio sweep conducted at 900 rpm using the specified kinetic mechanisms at spark timing conditions calculated from the TPA (i.e., 10.5±0.4 bar and 680±5 K - see Figure 22 in Appendix A - for all equivalence ratios and engine speeds). Notably, we observe significant variations in the flame speed across different equivalence ratios. For instance, the laminar flame speed at ϕ = 0.55 with Alekseev is calculated at 2.99 m/s, while at ϕ = 0.25, it drops to 3.5 cm/s, representing a nearly 100-fold difference. Despite this substantial disparity, the combustion duration between these conditions is relatively similar. It is important to acknowledge that kinetic mechanisms, although validated against experimental data, may not have been specifically validated at the high pressures and low equivalence ratios encountered in this study. Moreover, when dealing

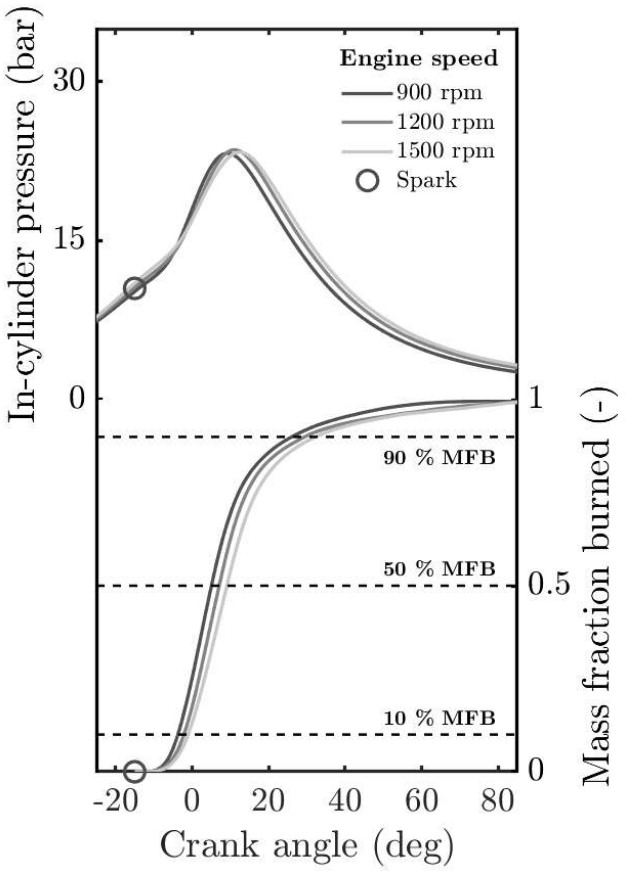

Figure 12: In-cylinder pressure and mass fraction burned (calculated from the TPA) as a function of the crank angle for 3 engine speeds (900, 1200 and 1500 rpm). P_2 = 0.7 bar and ST = -15 °aTDC.

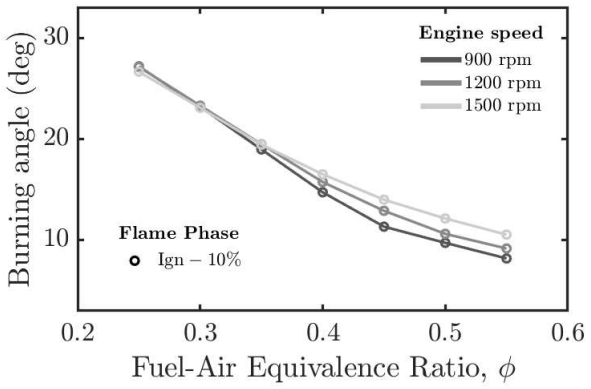

Figure 13: Combustion duration for the three engine speeds (in crank angle degrees) as a function of the fuel-air equivalence ratio with P_2 = 0.7 bar.

with hydrogen flames under such conditions, the presence of instabilities can significantly impact the measurement of flame speed and the calculation of the laminar flame speed [25]. As a result, there may be inherent uncertainties associated with the determination of flame speed in these operating regimes. Furthermore, it should be noted that different kinetic mechanisms exhibit significant differences in these conditions. Specifically, the flame speed is underestimated by approximately 40% across all equivalence ratios, and the flame thickness is overestimated by approximately 160% comparing GRI-Mech 3.0 to the Burke et al. and Alekseev et al. mechanisms. For the sake of simplicity, the Burke mechanism was used for the subsequent flame property analysis in this work.

Next, a dimensionless time, denoted as t^*, is defined to analyze the burning time while considering the flame properties. It is calculated

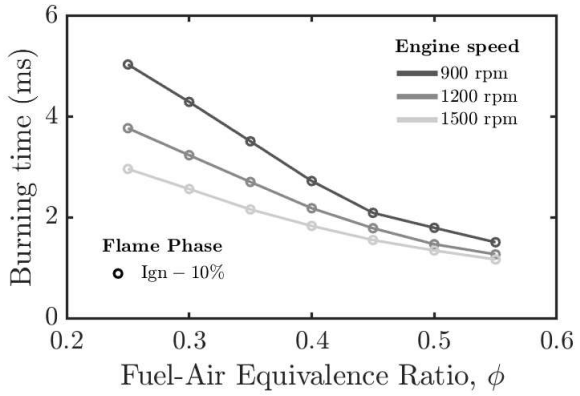

Figure 14: Combustion duration (in ms) for the three engine speeds (900, 1200 and 1500 rpm) as a function of the equivalence ratio.

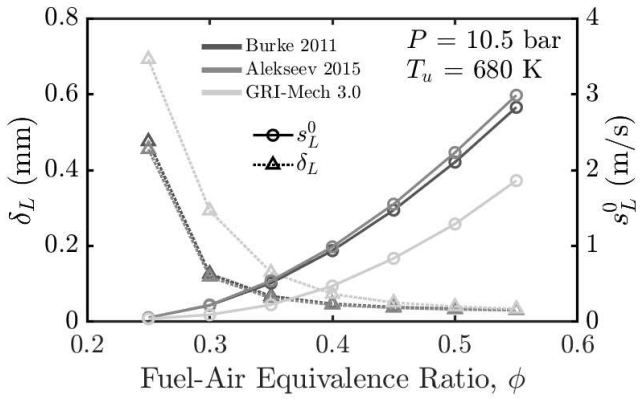

Figure 15: Laminar flame speed, s_L^0, and thickness, δ_L, as a function of the equivalence ratio calculated at the spark timing pressure and temperature conditions for the 900 rpm experiments.

using Equation 1:

$$t^* = \frac{t_{\Delta\theta}}{t_f} \tag{1}$$

where $t_{\Delta\theta}$ represents the time it takes for the mixture to burn 10% (in mass) after the spark timing. Figure 16 illustrates the dimensionless time, t^*, as a function of the fuel-air equivalence ratio.

The trend shows a non-linear relationship where the dimensionless time increases with higher fuel-air equivalence ratios, indicating thinner and faster flames. The influence of turbulence is evident, as a higher turbulent environment enhances flame speed and reduces combustion time. This leads to the question: how much is the ultra-lean hydrogen flame influenced by turbulence? To address this question, a classical approach based on turbulent intensity is employed to analyze turbulent flames. The turbulent flame speed, denoted as s_T, is determined using the Damköhler expression [26] outlined in Equation 2:

$$s_T = s_L \left(1 + \frac{u'}{s_L}\right) \tag{2}$$

where u' is the characteristic mean turbulent velocity fluctuation. This velocity can be estimated for the three engine speeds by considering the mean piston speed, $\overline{S_p}$, as described in Equation 3 [19, 27]. The turbulent velocity calculated for 900, 1200 and 1500 rpm are, respectively, 1.29, 1.71 and 2.14 m/s.

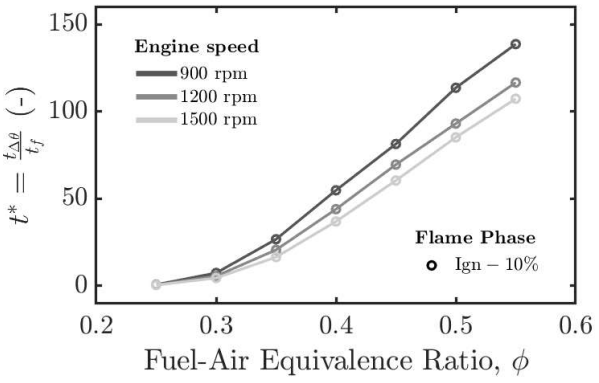

Figure 16: Dimensionless time, $t^* = t_{\Delta\theta}/t_f$, as a function of the fuel-air equivalence ratio.

$$u' \approx \frac{\overline{S_p}}{2} \tag{3}$$

Figure 17 depicts the dimensionless time, considering the influence of turbulent flame speed, as a function of the equivalence ratio. Notably, the ratio between physical burning time and chemical flame time for the three engine speeds converges onto a single curve, indicating that the increase in flame speed caused by turbulence is accurately captured by the Damköhler equation. Moreover, the trend exhibits a closer resemblance to a linear relationship with the equivalence ratio. This is evident from the increase in the coefficient of determination, which rises from 97.8% to 98.5% at 900 rpm.

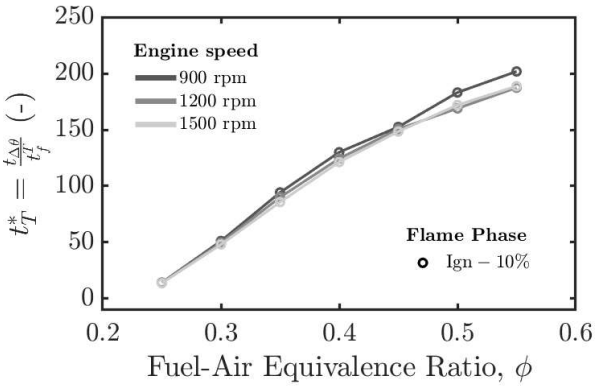

Figure 17: Dimensionless time taking into account the turbulent flame speed, $t_T^* = t_{\Delta\theta}/t_f^T$, as a function of the fuel-air equivalence ratio.

It is widely recognized that the hydrogen-air flame speed is influenced by both turbulence and intrinsic instabilities, such as thermodiffusive instabilities [4, 5, 12]. The impact of thermodiffusive instabilities on flame speed is contingent upon the equivalence ratio, pressure, and temperature, and efforts have been made to quantify this effect.

Darrieus and Landeau, in their pioneering works [28, 29], were among the first to predict the occurrence of unconditional instability in planar flames as a result of thermal expansion across the flame. To analyze this phenomenon, a flame surface that propagates at a speed s_L with a characteristic thickness δ_L is considered. The flame surface, F, can be described by the equation:

$$F(x,t) = A\exp(\omega t + ikx) \tag{4}$$

Here, ω represents the growth rate of the instability, and k denotes the wavenumber. The expression for the normalized growth rate,

known as the Darrieus-Landau expression, is given by [30]:

$$\tilde{\omega} = \omega \frac{\delta_L}{s_L} = \frac{1}{\sigma + 1} \left(\sqrt{\sigma^3 + \sigma^2 - \sigma} - \sigma \right) \tilde{k} = \omega_{DL} \tilde{k} \tag{5}$$

In this equation, σ represents the ratio of unburned and burned gas density (ρ_u/ρ_b), and the wavenumber is normalized by the flame thickness ($\tilde{k} = k\delta_L$). It is important to note that in combustion, the value of σ is typically greater than 1, resulting in a positive growth rate ω. This indicates that the flame is unstable for all wavenumbers.

However, studies have shown that this unconditional instability predicted by the Darrieus-Landau expression is not observed experimentally. To account for the stabilizing and destabilizing effects of diffusion across the flame, further research has been conducted [31, 32, 33]. As a result, a new model has been derived, which includes a second-order term in $\tilde{k}$, taking the form [34]:

$$\begin{aligned} \tilde{\omega} &= \omega_{DL} \tilde{k} - \left[B_1 + B_2 \beta (Le_{eff} - 1) B_3 Pr \right] \tilde{k}^2 \\ &= \omega_{DL} \tilde{k} + \omega_2 \tilde{k}^2 \end{aligned} \tag{6}$$

where B_i are constants that depend on the density ratio σ and the thermal conductivity. Additionally, β denotes the Zel'dovich number of the reaction, and Pr represents the Prandtl number. The coefficient ω_2 captures the effect of the second-order term. If ω_2 is negative, it results in an overall stabilizing effect, leading to a finite wavenumber beyond which flame waves are suppressed (thermodiffusive stability). Conversely, if ω_2 is positive, it indicates that the flame is unstable (thermodiffusive instability).

Recent studies calculated the ω_2 variable over a wide range of equivalence ratios, pressures and temperatures [35, 36, 12]. Figure 18 showcases contour plots from Hernandez et al. [12] (calculated with the Burke et al. [22] mechanism) illustrating the variation of ω_2 for different equivalence ratios and pressures at a temperature of 750 K, which is close to the in-cylinder conditions at spark timing.

The contour map of ω_2 reveals that higher positive values of ω_2 are observed at lower equivalence ratios ($0.2 < \phi < 0.5$) and within a pressure range of 0.5 to 6 MPa and negative (stabilizing the flame) at higher equivalence ratios and lower pressures. The red circles in the map represent the in-cylinder conditions for the experiments conducted at 900 rpm. This highlights the variation in flame acceleration under engine operating conditions. Specifically, at an equivalence ratio of 0.25, the ω_2 value exceeds 6, whereas at an equivalence ratio of 0.55, the ω_2 value approaches 0 under the same pressure and temperature conditions.

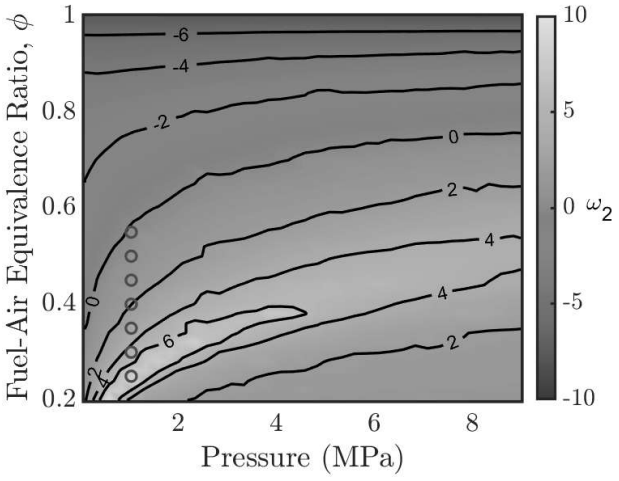

Figure 18: Map of the ω_2 variable over pressure and equivalence ratio for T = 750 K [12]. The red circles represent the cylinder conditions at spark timing for the 900 rpm experiments.

Equations 7 and 8 offer a method for estimating the flame speed enhancement and flame thickness variation using the instability parameter ω_2 [12, 36]:

$$\frac{s_F}{s_L} = \begin{cases} \exp(0.08\omega_2) & \text{if } P < \prod_c \\ 1 + 0.47\omega_2 & \text{otherwise} \end{cases} \tag{7}$$

$$\frac{\delta_F}{\delta_L} = \begin{cases} \exp(-0.06\omega_2) & \text{if } P < \prod_c \\ \frac{1}{1+0.26\omega_2} & \text{otherwise} \end{cases} \tag{8}$$

In this equation, s_F and δ_F are the flame speed and the thickness with instability effects, and s_L and δ_L, the laminar flame speed and thickness, respectively. The pressure criterion $\prod_c$ is calculated by the Equation 9 [35]:

$$\prod_c = \left(\frac{20\phi}{7 - 2\Theta} \right)^{150/(21+10\Theta)} \tag{9}$$

where Θ is the ratio between the unburned temperature and the reference temperature, T_{ref}, set to 300 K.

Considering the flame modification due to thermodiffusive instabilities and applying the Damköhler expression for turbulent combustion, it becomes possible to understand and attempt to correlate the engine burning time with hydrogen flame properties. Figure 19 provides a comparison of the dimensionless time, accounting for both thermodiffusive instabilities and turbulence enhancement, with the case where only turbulence is considered. This comparison helps in assessing the combined influence of these factors on the engine's combustion process.

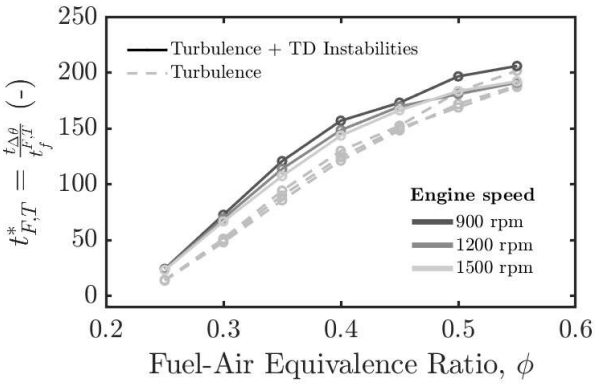

Figure 19: Dimensionless time accounting for the hydrogen flame acceleration due to thermodiffusive instabilities, $t^*_{F,T} = t_{\Delta\theta}/t_f^{F,T}$, as a function of the fuel-air equivalence ratio.

As expected, the presence of thermodiffusive instabilities reduces the chemical reaction time, leading to an increase in the dimensionless time compared to the curve without considering these instabilities (particularly at low equivalence ratios). However, the relationship between physical burning time and the chemical characteristic time of the flame is non-linear. Between equivalence ratios of 0.25 and 0.4, the trend appears to be linear, but beyond this range, the dimensionless time does not increase as much as the equivalence ratio. This observation indicates that there is an inter-correlation between turbulence and thermodiffusive instabilities that should be taken into account to fully understand their combined effects on the combustion process.

As discussed previously, it is important to exercise caution when considering laminar flame speeds at high pressures and low equivalence ratios, as well as in interpreting the results that take into account these factors, such as the values of u'/s_L and s_F/s_L. To gain insight into these quantities, Figure 20 illustrates u'/s_L, which quantifies the increase in flame speed due to turbulence according to the Damköhler expression, and the ratio of flame speed enhancement attributable to thermodiffusive instabilities, denoted as s_F/s_L.

The ratio u'/s_L exhibits an exponential growth as the equivalence ratio decreases, with values ranging from approximately 30 to 40 at $\phi = 0.25$. This significant variation is not commonly observed with conventional fuels, which tend to exhibit minimal changes in laminar flame speeds across different operating equivalence ratios when compared to hydrogen. Furthermore, the flame speed enhancement resulting from TD instabilities varies between 1.01 and 1.10 at high equivalence ratios ($\phi = 0.55$ and 0.45, respectively), and between 1.94 and 1.46 at low equivalence ratios ($\phi = 0.25$ and 0.3, respectively). These results provide quantitative insight into the influence of turbulence and instabilities on flame behavior in internal combustion engines, particularly at low load conditions.

Finally, investigating of the impact of intake pressure on hydrogen flame properties, Figure 21 displays the dimensionless time for the three engine speeds as a function of equivalence ratio, considering two intake pressures (P_2 = 0.7 and 0.9 bar). It can be observed

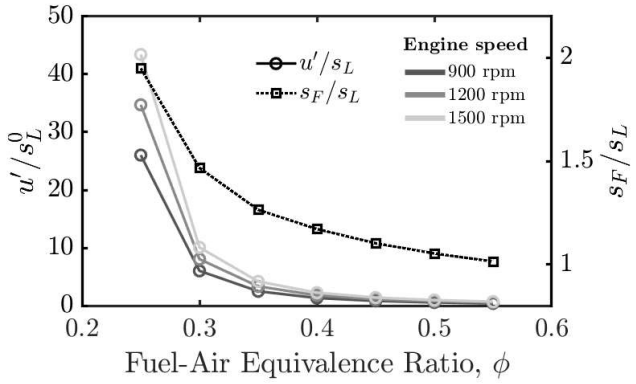

Figure 20: u'/s_L and s_F/s_L as a function of the equivalence ratio for the three engine speeds at 0.7 bar of intake pressure.

that at higher pressures, the combustion durations slightly decrease, indicating faster combustion. Additionally, the laminar flame speed increases with higher intake pressures. So, dimensionless time exhibits an increase, particularly at higher equivalence ratios. This increase brings the trend closer to linearity, suggesting a more direct correlation between physical burning time and the chemical characteristic time of the flame. However, it should be noted that equivalence ratios beyond 0.4 start to deviate from this trend.

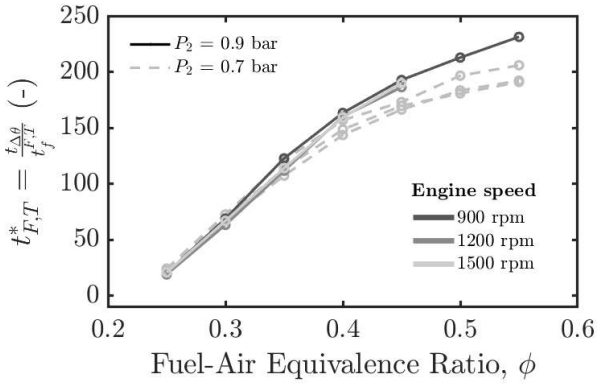

Figure 21: Dimensionless time accounting for the hydrogen flame acceleration due to thermodiffusive instabilities and turbulence for two intake pressures (P_2 = 0.7 and 0.9 bar) as a function of the fuel-air equivalence ratio.

The analysis reveals that the position of the maximum point of instability shifts as the equivalence ratio varies, especially when considering different pressures at the time of the spark. It is observed in Figure 18 that higher pressures result in the maximum instability occurring at higher equivalence ratios. This relationship is well captured by the curve in Figure 21, since the bend on the curve after a linear trend at lower equivalence ratio happens at a higher equivalence ratio (ϕ = 0.45). For higher values, the bending suggests that additional factors or phenomena not accounted for in the current model may come into play, influencing the combustion behavior in these conditions. Further investigation and refinement of the flame model may be necessary to accurately capture the combustion characteristics at higher equivalence ratios. Especially, accurate prediction of laminar flame speed.

CONCLUSION

Experiments were conducted using a single-cylinder gasoline baseline internal combustion engine that was converted to operate with hydrogen fuel. The fuel-air equivalence ratio (ϕ) was set to vary from 0.25 to 0.55. The experimental data obtained from these tests was then analyzed using the Three Pressure Analysis (TPA) model in GT-Power. The main findings are stated below:

- 0D/1D simulators prove to be valuable tools for studying hydrogen-fueled engines. These tools offer the advantage of a more accurate heat transfer analysis, allowing for the extraction of consistent net heat release and mass fraction burned traces.

- Minimal cyclic variations were observed in the operation of a homogeneous mixture ultra-lean hydrogen-air internal combustion engine. Cyclic variations, primarily attributed to misfires, were identified at fuel-air equivalence ratios below 0.2.
- The fuel-air equivalence ratio significantly influences flame initiation, while its impact on flame propagation and the end-flame phase is less pronounced.
- The combustion duration is correlated to the chemical characteristic time of the hydrogen flame, but no direct relationship is found, possibly due to inter-correlations between turbulence and thermodiffusive instabilities.
- The laminar flame speed obtained from kinetic mechanisms calculations at spark timing in internal combustion engines should be approached with caution, especially for ultra-lean mixtures and high in-cylinder pressures. The disparity in flame speed obtained from kinetic mechanisms is substantial, differing by nearly 100 times. In contrast, experimental measurements show a relatively small variation in combustion duration, ranging from 73.9 CAD to 27.1 CAD for the 10 to 90% MFB range, respectively, between ϕ = 0.25 and 0.55, under the same operating conditions (P_2 = 0.7 bar, ST = -15 °aTDC, and 900 rpm).

Optical analysis of the hydrogen flame would provide valuable insights into flame development and the underlying physics within the cylinder (e.g. the flame radius growth as function of the crank angle for multiple conditions, instabilities visualization, and repeatability of the flame over the cycles). Further investigations focusing on hydrogen-air mixture formation, flow field analysis, turbulence characterization, and flame visualization would enhance the understanding of in-cylinder hydrogen flame behavior.

DECLARATION OF COMPETING INTEREST

The authors declare that they have no known competing financial interests or personal relationships that could have appeared to influence the work reported in this paper.

ACKNOWLEDGEMENTS

The authors gratefully acknowledge the generous support of the Agence Nationale de Recherche under grant number 20-CE05-0007 (ALEKCIA ANR project). The authors also extend their gratitude to Realis Simulation Ltd. for providing the ω_2 map used in the thermodiffusive flame analysis.

REFERENCES

[1] S. Verhelst and T. Wallner, "Hydrogen-fueled internal combustion engines," *Progress in Energy and Combustion Science*, vol. 35, no. 6, pp. 490–527, 2009.

[2] D. G. Caglayan, H. U. Heinrichs, M. Robinius, and D. Stolten, "Robust design of a future 100% renewable european energy supply system with hydrogen infrastructure," *International Journal of Hydrogen Energy*, vol. 46, no. 57, pp. 29376–29390, 2021.

[3] K. Truffin, C. Angelberger, S. Richard, and C. Pera, "Using large-eddy simulation and multivariate analysis to understand the sources of combustion cyclic variability in a spark-ignition engine," *Combustion and Flame*, vol. 162, no. 12, pp. 4371–4390, 2015.

[4] L. Berger, A. Attili, and H. Pitsch, "Intrinsic instabilities in premixed hydrogen flames: parametric variation of pressure, equivalence ratio, and temperature. part 2 – non-linear regime and flame speed enhancement," *Combustion and Flame*, vol. 240, p. 111936, 2022.

[5] L. Berger, A. Attili, and H. Pitsch, "Synergistic interactions of thermodiffusive instabilities and turbulence in lean hydrogen flames," *Combustion and Flame*, vol. 244, p. 112254, 2022.

[6] C. Ramalho Leite, R. Oung, P. Brequigny, J. Borée, and F. Foucher, "Combustion cycle-to-cycle variation analysis in diesel baseline hydrogen-fueled spark-ignition engines," in *WCX SAE World Congress Experience*, SAE International, 2023.

[7] Y. Kim, J. T. Lee, and G. H. Choi, "An investigation on the causes of cycle variation in direct injection hydrogen fueled engines," *International Journal of Hydrogen Energy*, vol. 30, no. 1, pp. 69–76, 2005.

[8] F. Ma, H.-Q. Liu, Y. Li, Y. Wang, and S.-L. Zhao, "Analysis of in-cylinder combustion of hydrogen fueled engine," *Chinese Internal Combustion Engine Engineering*, vol. 29, pp. 29–33, 2008.

[9] X. yu Li, B. gang Sun, D. sheng Zhang, X. Wang, L. zhi Bao, and Q. he Luo, "Experimental study on the cycle variation characteristics of direct injection hydrogen engine," *Energy Conversion and Management: X*, vol. 15, p. 100260, 2022.

[10] Y. Chen, "Stability research of hydrogen internal combustion engine in idle condition," master's thesis, Beijing Institute of Technology, 2008.

[11] B. Sun, D. Zhang, and F. Liu, "Cycle variations in a hydrogen internal combustion engine," *International Journal of Hydrogen Energy*, vol. 38, no. 9, pp. 3778–3783, 2013.

[12] I. Hernandez, C. Turquand d'Auzay, R. Penning, E. Shapiro, and J. Hughes, "Thermo-diffusive flame speed adjustment and its application to hydrogen engines," in *WCX SAE World Congress Experience*, SAE International, 2023.

[13] GT-SUITE, *Engine Performance Application Manual*. Gamma Technologies.

[14] S. Choi, C. P. Kolodziej, A. Hoth, and T. Wallner, "Development and validation of a three pressure analysis (tpa) gt-power model of the cfr f1/f2 engine for estimating cylinder conditions," in *WCX World Congress Experience*, SAE International, 2018.

[15] G. Maio, A. Boberic, L. Giarracca, D. Aubagnac-Karkar, O. Colin, F. Duffour, K. Deppenkemper, L. Virnich, and S. Pischinger, "Experimental and numerical investigation of a direct injection spark ignition hydrogen engine for heavy-duty applications," *International Journal of Hydrogen Energy*, vol. 47, no. 67, pp. 29069–29084, 2022.

[16] E. Monemian, "Simulating diesel-hydrogen combustion by gt-power," 10 2018.

[17] F. Millo, A. Piano, L. Rolando, F. Accurso, F. Gullino, S. Roggio, A. Bianco, F. Pesce, A. Vassallo, and R. Rossi, "Synergetic application of zero-, one-, and three-dimensional computational fluid dynamics approaches for hydrogen-fuelled spark ignition engine simulation," *SAE International Journal of Engines*, vol. 15, pp. 561–580, dec 2021.

[18] J. Demuynck, M. De Paepe, H. Huisseune, R. Sierens, J. Vancoillie, and S. Verhelst, "On the applicability of empirical heat transfer models for hydrogen combustion engines," *International Journal of Hydrogen Energy*, vol. 36, no. 1, pp. 975–984, 2011. 11th International Conference: "Hydrogen Materials Science & Chemistry of Carbon Nanomaterials".

[19] J. Heywood, *Internal Combustion Engine Fundamentals*. Automative technology series, McGraw-Hill Education, 1988.

[20] N. Ozdor, M. Dulger, and E. Sher, "Cyclic variability in spark ignition engines - a literature survey," *SAE Technical Papers*, no. 940987, 1994.

[21] K. J. Richards, P. K. Senecal, and E. Pomraning, "Converge cfd software (v3.0)," 2020.

[22] M. P. Burke, M. Chaos, Y. Ju, F. L. Dryer, and S. J. Klippenstein, "Comprehensive h2/o2 kinetic model for high-pressure combustion," *International Journal of Chemical Kinetics*, vol. 44, no. 7, pp. 444–474, 2012.

[23] V. A. Alekseev, M. Christensen, and A. A. Konnov, "The effect of temperature on the adiabatic burning velocities of diluted hydrogen flames: A kinetic study using an updated mechanism," *Combustion and Flame*, vol. 162, no. 5, pp. 1884–1898, 2015.

[24] G. P. Smith, D. M. Golden, M. Frenklach, N. W. Moriarty, B. Eiteneer, M. Goldenberg, C. T. Bowman, R. K. Hanson, S. Song, W. C. G. Jr., V. V. Lissianski, and Z. Qin. http://combustion.berkeley.edu/gri-mech/.

[25] W. Kim, Y. Sato, T. Johzaki, T. Endo, D. Shimokuri, and A. Miyoshi, "Experimental study on self-acceleration in expanding spherical hydrogen-air flames," *International Journal of Hydrogen Energy*, vol. 43, no. 27, pp. 12556–12564, 2018.

[26] H. S. Awad, K. Abo-Amsha, U. Ahmed, M. Klein, and N. Chakraborty, "Assessment of Damköhler's hypotheses in the thin reaction zone regime using multi-step chemistry direct numerical simulations of statistically planar turbulent premixed flames," *Physics of Fluids*, vol. 34, 05 2022.

[27] J. Borée and P. Miles, "In-cylinder flow," *in D. Crolla, D.E. Foster, T. Kobayashi and N. Vaughan (Eds.), Encyclopedia of Automotive Engineering*, 04 2014.

[28] G. Darrieus, "Propagation d'un front de flamme," *La Technique Moderne*, vol. 30, p. 18, 1938.

[29] L. Landau, "On the theory of slow combustion," in *Dynamics of Curved Fronts* (P. Pelcé, ed.), pp. 403–411, San Diego: Academic Press, 1988.

[30] C. Law and C. Sung, "Structure, aerodynamics, and geometry of premixed flamelets," *Progress in Energy and Combustion Science*, vol. 26, no. 4, pp. 459–505, 2000.

[31] M. L. Frankel and G. I. Sivashinsky, "The effect of viscosity on hydrodynamic stability of a plane flame front," *Combustion Science and Technology*, vol. 29, no. 3-6, pp. 207–224, 1982.

[32] P. Pelce and P. Clavin, "Influence of hydrodynamics and diffusion upon the stability limits of laminar premixed flames," *Journal of Fluid Mechanics*, vol. 124, p. 219–237, 1982.

[33] M. Matalon and B. J. Matkowsky, "Flames as gasdynamic discontinuities," *Journal of Fluid Mechanics*, vol. 124, p. 239–259, 1982.

[34] M. MATALON, C. CUI, and J. K. BECHTOLD, "Hydrodynamic theory of premixed flames: effects of stoichiometry, variable transport coefficients and arbitrary reaction orders," *Journal of Fluid Mechanics*, vol. 487, p. 179–210, 2003.

[35] T. Howarth and A. Aspden, "An empirical characteristic scaling model for freely-propagating lean premixed hydrogen flames," *Combustion and Flame*, vol. 237, p. 111805, 2022.

[36] T. Howarth, E. Hunt, and A. Aspden, "Thermodiffusively-unstable lean premixed hydrogen flames: Phenomenology, empirical modelling, and thermal leading points," *Combustion and Flame*, vol. 253, p. 112811, 2023.

APPENDIX A. SUPPLEMENTARY DATA

Unburned Gas Temperature

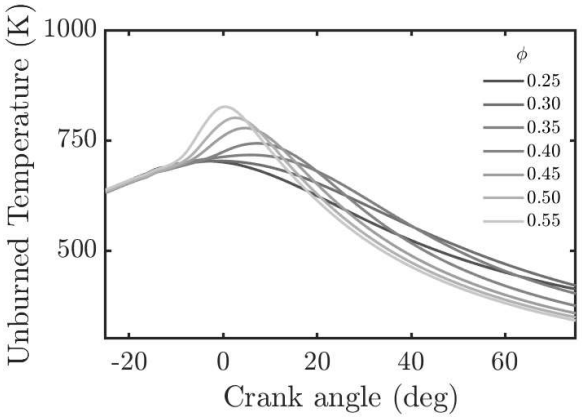

Figure 22: Unburned gas temperature as a function of the crank angle for 7 equivalence ratios at 900 rpm and P_2 = 0.7 bar. The spark timing is -15 °aTDC.

DEFINITIONS/ABBREVIATIONS

β	Zel'dovich Number
δ_F	Thermodiffusive Flame Thickness
δ_L	Laminar Flame Thickness
$\Delta\theta$	Combustion Duration
ϕ	Fuel-Air Equivalence Ratio
λ	Air-Fuel Equivalence Ratio
$\prod_c$	Pressure Criterion
σ	Gas Density Ratio
Θ	Temperature Ratio
ω	Instability Growth Rate
ω_2	Second Order Instability Coefficient
ω_{DL}	First Order Instability Coefficient
F	Flame surface
k	Wavenumber
P_2	Mean Intake Pressure
P_3	Mean Exhaust Pressure
Pr	Prandtl Number
$\overline{S_p}$	Mean Piston Speed
s_F	Thermodiffusive Flame Speed
s_L	Laminar Flame Speed
s_L^0	Un-stretched Laminar Flame Speed
s_T	Turbulent Flame Speed
t^*	Dimensionless Time (Laminar Flame)
t_T^*	Dimensionless Time (Turbulent Flame)
$t_{F,T}^*$	Dimensionless Time (Turbulent and TD Flame)
$t_{\Delta\theta}$	Time to Burn 10% of Fuel Mass
t_f	Characteristic Flame Time
t_f^T	Characteristic Turbulent Flame Time
$t_f^{F,T}$	Characteristic Turbulent and TD Flame Time
T_2	Mean Intake Temperature
T_{ref}	Reference Temperature
u'	Characteristic Mean Turbulent Velocity Fluctuation
°aTDC	Crank Angle Degree After Firing Top Dead Center
CAD	Crank angle degrees
CCV	Cycle-to-cycle variation
CoV	Coefficient of variation
DoE	Design of Experiments
gIMEP	Gross Indicated Mean Effective Pressure
GT	Gamma Technologies
$\mathbf{H}_2$	Hydrogen
HRR	Heat Release Rate
ICE	Internal Combustion Engine
IMEP	Indicated Mean Effective Pressure
MFB	Mass Fraction Burned
NOx	Nitrogen Oxides
rpm	Rotation per Minute
ST	Spark Timing
TD	Thermodiffusive
TDC	Top Dead Center
TPA	Three Pressure Analysis